

# Identification of specific inhibitors of *Trypanosoma cruzi* Malic Enzyme isoforms by target-based HTS.

Americo T. Ranzani,<sup>1,2</sup> Cristina Nowicki<sup>3</sup>, Shane R. Wilkinson<sup>4</sup>, Artur T. Cordeiro<sup>1,\*</sup>

<sup>1</sup> Brazilian Biosciences National Laboratory, Brazilian Center for Research in Energy and Materials, Campinas, SP, Brazil

<sup>2</sup> Institute of Biology, University of Campinas, Campinas, SP, Brazil

<sup>3</sup> Facultad de Farmacia y Bioquímica, Instituto de Química y Fisicoquímica Biológica (IQUIFIB-CONICET), Universidad de Buenos Aires, Buenos Aires, Argentina

<sup>4</sup> School of Biological and Chemical Sciences, Queen Mary University of London, London, United Kingdom

\* corresponding author Tel.: +55 19 35121121; fax: +55 19 35121006 E-mail address: [artur.cordeiro@lnbio.cnpem.br](mailto:artur.cordeiro@lnbio.cnpem.br).

**KEYWORDS:** Malic Enzyme, *Trypanosoma cruzi*, Chagas Disease, sulfonamides, HTS.

## **Abstract:**

*Trypanosoma cruzi* is the causative agent of Chagas disease. The lack of an efficient and safe treatment supports the research into novel metabolic targets, with the malic enzyme (ME) representing one such potential candidate. *T. cruzi* expresses a cytosolic (TcMEc) and a mitochondrial (TcMEm) ME isoform, with these activities functioning to generate NADPH, a key source of reducing equivalents that drives a range of anabolic and protective processes. To identify specific inhibitors that target TcMEs, two independent high-throughput screening strategies using a diversity library containing 30,000 compounds were employed. IC<sub>50</sub> values of 262 molecules were determined for both TcMEs as well as for three human ME isoforms, with the inhibitors clustered into six groups according to their chemical similarity. The most potent hits belonged to a sulfonamide group that specifically target TcMEc. Moreover, several selected inhibitors of both TcMEs showed trypanocidal effect against the replicative forms of *T. cruzi*. The chemical diversity observed among those compounds that inhibit TcMEs activity emphasizes the druggability of these enzymes, with a sulfonamide-based subset of compounds readily able to block TcMEc function at a low nanomolar range.

## Introduction

American trypanosomiasis, also known as Chagas disease, is caused by the protozoan *Trypanosoma cruzi*. According to the WHO, up to 7 million people across Latin America are infected by this pathogen, with the disease now emerging as a problem at non-endemic sites<sup>1,2</sup>. The available treatments are based on the use of two nitroheterocycle prodrugs, nifurtimox and benznidazole. Although less toxic than nifurtimox, benznidazole displays side effects leading to discontinuation of treatment by around 30% patients<sup>3,4</sup>. These prodrugs are curative against the initial acute stage of the disease with strains refractory to therapy being frequently encountered<sup>5,6</sup>. The use of benznidazole in chronic phase is still under investigation.<sup>7,8</sup> Against this backdrop there is a need for the development of safer, efficacious drug treatments that target all stages of the disease.

Reduced nicotinamide adenine dinucleotide phosphate (NADPH) has a crucial role in parasite survival. This co-factor is used as source of reducing equivalents to maintain trypanothione, the main free thiol found within this organism, in its reduced dihydro state. In this form trypanothione can drive a series of redox cascades that facilitate the detoxification of reactive oxygen species (ROS) produced from endogenous metabolic reactions or from exogenous immune insults generated by mammalian host cells<sup>9</sup>. Additionally, NADPH participates in a number of biosynthetic pathways, such as in fatty acid and nucleic acid synthesis<sup>10</sup>. As this co-factor plays an essential role in maintaining the reduced environment found within a cell and in the production of the basic building blocks required for cell viability, enzymes responsible for its generation are considered potential drug targets. In most organisms, the enzymes responsible for NADPH

production depend on intermediates derived from highly reduced substrates or with high energy-content. For instance, this is the case of the pentose-phosphate pathway (PPP)<sup>11</sup>, which includes the reactions catalyzed by glucose-6-phosphate dehydrogenase (G6PDH), and 6-phosphogluconate dehydrogenase (6PGDH). The operability of this route relies on the supply of glucose-6-phosphate (G6P) to maintain the flux of NADPH generation. On the other hand, enzymes such as malic enzymes (MEs)<sup>12</sup>, isocitrate dehydrogenase (IDH)<sup>13</sup> and glutamate dehydrogenase (GLDH)<sup>14</sup> also represent important candidates for NADPH production, mainly when glucose is scarce and amino acids are utilized as alternative source for energy production<sup>15</sup>.

*T. cruzi* energy metabolism changes according to the carbon source available in the different microenvironments the parasite finds itself during its life cycle<sup>16</sup>. In the infectious, non-replicative bloodstream trypomastigote form, the parasite is able to utilize the abundant glucose supply found in its mammalian host's bloodstream. In contrast, the replicative intracellular amastigotes grow in almost free glucose medium, and are predicted to depend on amino acids catabolism for energy production. Considering the nutrient availability in the amastigotes stage, enzymes such as ME, IDH and GDH are likely to gain importance in NADPH production.

Malic enzyme, in the presence of a divalent cation ions ( $Mg^{2+}$  or  $Mn^{2+}$ ), catalyzes the oxidative decarboxylation of malate to pyruvate, concomitantly reducing  $NAD(P)^+$  to  $NAD(P)H$ . *T. cruzi* and *T. brucei* expresses two ME isoforms, one located in the cytosol (TcMEc and TbMEc, respectively) and the other present in the mitochondrion (TcMEM and TbMEM, respectively)<sup>12</sup>. Down regulation of TbMEM expression using RNAi on *T. brucei* procyclic forms, the parasite stage found in the insect vector, has revealed that this isoform is essential for parasite survival whereas TbMEc along with the PPP is

responsible for NADPH production in the cytosol<sup>17</sup>. In *T. cruzi*, there is no information regarding the essentiality of the distinct ME isoforms. Although TcMEc and TbMEc catalyze the same reaction, both isozymes differ in their kinetic properties. TcMEc is allosterically activated by L-aspartate, a property that does not extend to the *T. brucei* counterpart. The allosteric regulation of TcMEc may reflect a relevant function of this isoform in *T. cruzi* metabolism.

Herein, we present the discovery of 262 novel TcMEc and TcMEem inhibitors identified using a biochemical high-throughput screen (HTS). Based on their structure, most (250) were placed into 6 distinct chemical classes, while the remainder represent structurally unrelated compounds (singletons). Different compounds specifically targeted TcMEc or TcMEem without significantly affecting the activity of human ME isoforms, with several displaying a growth inhibition effect against cultured *T. cruzi* epimastigotes and amastigotes.

## **Materials and Methods**

### **Chemicals**

The screening library DIVERSet™ and the resupply compounds were purchased from Chembridge. *Clostridium kluveri* diaphorase was obtained from Worthington Biochemical while resazurin, NADP<sup>+</sup>, NADPH, L-malic acid, L-aspartic acid, fumaric acid, MnCl<sub>2</sub> and DMSO were purchased from Sigma-Aldrich. Tris-HCl and NaCl were acquired from Merck and Triton X-100 was purchased from Serva. Microplates were bought from Greiner Bio-One.

## HsME expression constructs

DNA fragments encoding for HsME1 (NM\_002395), HsME2 (NP\_002387) and HsME3 (NM\_001161586) were amplified from MDA-mB-231 breast cancer (for HsME1 and HsME3) or human fetal brain (for HsME2) cDNA using the primers GCGGATCCCATATGGAGCCCGAAGCCC and GCCTCGAGCTACTGGTCAACTTTGG TCTGTATTTTCTGC for HsME1, GCGGATCCCATATGTTGCACATAAAAGAAAAAGG CAAGCC and GCCTCGAGCTATTCTGTTATCACAGGAGGGCTTG for HsME2 and GCGAGCTCCATATGGTGCCCCTGAAGAAGCGC and GCCTCGAGTCAGACCGTCT GAACATTCATGGC for HsME3 (underlined sequences correspond to restriction sites incorporated into the oligonucleotides to facilitate cloning). For HsME2 and HsME3, the amplified fragments lacked regions that encode for the first 18 or 44 amino acids, respectively, sequences predicted to contain a mitochondrial target peptide (MTP)<sup>18,19</sup>: The MTP sequence for HsME3 was predicted using MitoPROII v.1.101 (<http://ihg.gsf.de/ihg/mitoprot.html>). The human ME amplicons were cloned into the pGEM-T vector (Promega), sequenced before being subcloned into the NdeI and XhoI restriction sites of pET28a<sup>+</sup>.

## Protein expression and purification

The TcMEs heterologous expression followed the protocol published elsewhere<sup>12</sup>. In the case of HsMEs, *E. coli* Rossetta (DE3) pLysS containing the expression vector (pET28\_HsME1, pET28\_HsME2 or pET28\_HsME3) was cultured in the autoinduction ZYM5052 medium<sup>20</sup>, in the presence of 30 µg/mL kanamycin and 34 µg/mL chloramphenicol, at 22 °C for 60 hours. The cells were harvested and the pellets stored at -20°C.

The purification steps were the same for TcMEs and HsMEs. Cells were resuspended in buffer A (50 mM Tris-HCl pH 8.0, 500 mM NaCl) containing 5 mM imidazole and lysozyme (1 mg/mL). Following sonication, the clarified lysates were passed through a HisTrap HP column (GE Healthcare Life Technologies) and proteins eluted using an imidazole gradient (5 to 400 mM) in buffer A. ME-containing fractions were pooled and the proteins concentrated. The histidine tag was removed with thrombin (2 U/mg), for 16 hours at 4°C. Finally, the proteins were subjected to size exclusion chromatography on a Superdex 200 16/60 column (GE Healthcare Life Technologies) equilibrated with GF buffer (50 mM Tris-HCl pH 8.0, 150 mM NaCl). Purified proteins were concentrated using an Amicon Ultra-15 Centrifugal Filter device of 30 kDa molecular weight cutoff (Millipore) and stored at -80°C with 5% (v/v) glycerol.

### **Kinetic characterization**

The malate oxidative decarboxylation activities of recombinant MEs were assayed in a coupled reaction using diaphorase and resazurin (Fig 1A). In this system, NADPH generated during the ME-catalyzed conversion of malate to pyruvate is utilized by diaphorase to drive reduction of resazurin to resorufin. Resorufin production can then be followed by monitoring the change in fluorescence using a plate reader set to an excitation  $\lambda = 570$  nm and an emission  $\lambda = 590$  nm. The apparent Michaelis-Menten constant ( $K_m^{app}$ ) for NADP<sup>+</sup> or malate was determined by varying the concentration of one of the substrates while keeping the other at a saturating level. The activation constant ( $K_a$ ) of aspartate for TcMEc was determined as previously described<sup>21</sup>. All the reactions were performed at 25°C in Reaction Buffer (50 mM Tris-HCl pH 7.5, 50 mM NaCl and 0.01%

(v/v) Triton X-100) supplemented with 2 mM MnCl<sub>2</sub>, 10 μM resazurin and 2 U/mL diaphorase, in 384-well black v-bottom microplates and a final volume of 50 μL. The resorufin fluorescence intensity was measured using an EnVision plate reader (PerkinElmer).

### **Automated primary HTS**

The automated HTS assay for TcMEc and TcMEem was performed using the coupled system of diaphorase and resazurin, adapted from a previous reported dehydrogenase HTS assay<sup>22</sup>. The activity of either trypanosomal enzyme in the presence of a diversity chemical library of 29,760 compounds was assessed using a homogeneous end-point assay in 384-well plate format and performed in an automated workstation (liquid handler - JANUS-MDT, plate reader - EnVision – all from PerkinElmer). First, 22 μL Reaction Mix was added into the wells, followed by the transfer of 0.5 μL sample compound (stock at 1 mM in 100% (v/v) DMSO). The reaction was then initiated by addition of 2.5 μL malate (concentrations are described below). Following incubation at room temperature for 3 hours, the end-point fluorescence intensity of resorufin was measured (excitation  $\lambda$  =570 nm, emission  $\lambda$  =590 nm). The Final Assay Concentration (FAC) of reagents for assaying TcMEem activity was as follows: 10 μM NADP<sup>+</sup>, 2 mM MnCl<sub>2</sub>, 10 μM resazurin, 1 U/mL diaphorase, 63 pM TcMEem and 1 mM malate. All plates contained 32 positive controls (Reaction Mix + DMSO + malate) and 32 negative controls (Reaction Mix + DMSO + Reaction Buffer). The fluorescence intensity readouts were normalized, considering the means of positive and negative controls in each plate as 100% and 0% of reminiscent activity (RA), respectively. The assay quality was evaluated by the Z-factor<sup>23</sup>. The



compounds with RA less than or equal to the cutoff RA was considered a hit candidate. The cutoff RA was defined as the average RA of all samples minus three standard deviation. For TcMEc-based reactions, the above assay was performed in the presence of L-aspartate (FAC = 400  $\mu$ M) and using different concentrations of TcMEc (FAC = 25  $\mu$ M), NADP<sup>+</sup> (FAC = 20  $\mu$ M) and malate (FAC = 1.3 mM).

### **Confirmation Assay**

The hit candidates were assayed against TcMEs and against diaphorase only, to exclude false positives and inhibitors of the coupled system. The hit candidates were transferred from the screening library plates to new assay plates and assayed in triplicate, monitoring the resorufin formation for 30 minutes. The calculated velocities were normalized using controls. For TcMEs, the assay conditions were the same for HTS assay, except 2x amount of enzyme (TcMEs and diaphorase) was used. For diaphorase only reactions, the assay concentration of reagents was 15  $\mu$ M NADPH, 2 mM MnCl<sub>2</sub>, 10  $\mu$ M resazurin, 0.035 U/mL diaphorase.

### **IC<sub>50</sub> determination**

Initially, the effect of a single dose (80  $\mu$ M) of hit compound against TcMEs, HsMEs and diaphorase was assessed. For those structures that inhibited ME function by > 50% without affecting diaphorase, the concentration of compound that inhibited ME activity (IC<sub>50</sub>) by 50% was determined. First, the selected compounds were serially diluted (2.5-fold dilution steps) in DMSO using a Versette Automated Liquid Handler (ThermoFischer Scientific). Next, the Reaction Mix and compounds were dispensed in 384-well plates using the Versette Automated Liquid Handler and the reaction was initiated with malate

using MultidropCombi Reagent Dispenser (ThermoFischer Scientific). The FAC for each compound were 80, 32, 12.8, 5.12, 2.05, 0.82, 0.328, 0.13, 0.052, 0.021, 0.008 and 0  $\mu$ M. The velocity of resorufin formation was followed using a Clariostar microplate reader (BMG LABTECH), following manufacturer instructions for resorufin fluorescence (excitation  $\lambda$  = 545 nm; emission  $\lambda$  = 600 nm). The data were normalized with controls and analyzed in GraphPad Prism 5, using a sigmoidal curve.

For TcMEs, the reagents concentrations were the same used in the Confirmation Assay, while for human MEs, the above inhibition assays were performed using 6  $\mu$ M NADP<sup>+</sup> and 4.7 mM malate for HsME1 (2.5 nM)-based assay; 1 mM NADP<sup>+</sup>, 0.7 mM fumarate and 4.5 mM malate in reactions containing HsME2 (12.5 nM) and 10  $\mu$ M NADP<sup>+</sup> and 3.4 mM malate were used when testing HsME3 (1.25 nM): all the reaction mixtures contained 2 mM MnCl<sub>2</sub>, 10  $\mu$ M resazurin and 1 U/mL diaphorase.

### **Mechanism of inhibition**

The mechanism of inhibition was established for TcMEs, by determining the Michaelis-Menten saturation curves for malate or NADP<sup>+</sup> in the presence of 4 different concentrations of inhibitor, and with DMSO as control. This enzyme was used because its activity is not effected by L-aspartate while the inhibitors analysed exhibited inhibition for either TcMEs. The resultant curves were fitted to non-linear inhibition model by using GraphPad Prism 5 (GraphPad Software) from which the apparent inhibition constant  $K_i^{APP}$  was obtained. The inhibitory mechanism was considered the one with the model with the higher  $r^2$  (> 0.98). The Lineweaver-Burk plots were also used to qualitatively assess the inhibitory mechanism and data representation.

## Cell culture

The L6 rat myoblast cell line was cultured at 37°C under a 5% (v/v) CO<sub>2</sub> atmosphere in RPMI-1640 supplemented with 5 g/L HEPES pH 8.0, 0.34 g/L sodium glutamate, 0.22 g/L sodium pyruvate, 2500 U/L penicillin, 0.25 g/L streptomycin and 10% (v/v) heat inactivated foetal calf serum.

The *T. cruzi* (strain Y) epimastigote cells were grown at 27°C in Liver Infusion Tryptose medium<sup>24</sup> supplemented with 10% (v/v) heat inactivated foetal calf serum. *T. cruzi* (strain Sylvio X10/6) epimastigotes engineered to express the thermostable red-shifted firefly luciferase (PpyRE9h)<sup>25</sup> were cultured at 27°C in RPMI-1640 containing 5 g/L trypticase, 20 mg/L heamin, 5 g/L HEPES pH 8.0, 0.34 g/L sodium glutamate, 0.22 g/L sodium pyruvate, 2500 U/L penicillin, 0.25 g/L streptomycin and 10% (v/v) heat inactivated foetal calf serum. Infection of L6 monolayers with recombinant *T. cruzi* and the culturing of amastigote parasites was carried out as previously described<sup>26</sup>.

## Antiproliferative assays

All assays were performed in a 96-well plate format. To determine mammalian cytotoxicity, growth medium (200 µL) containing 1500 L6 cells and different concentrations of compound (80 to 0.82 µM) were incubated at 37°C for 96 hours. Resazurin (FAC = 50 µM) was added to each well and cultures incubated for a further 6 hours. The fluorescence of each culture was determined using a Gemini fluorescent plate reader (Molecular Devices) (excitation  $\lambda$  = 530 nm, emission  $\lambda$  = 585 nm, filter cutoff at

550) with the change in fluorescence resulting from the reduction of resazurin to resorufin being proportional to the number of live cells. The compound concentration that inhibits cell growth by 50% ( $EC_{50}^{L6}$ ) was established using the non-linear regression tool on GraphPad Prism 5 (GraphPad Software).

Growth inhibition assays against *T. cruzi* (strain Y) epimastigotes was performed using the CellTiter 96<sup>®</sup> AQueous One Solution Cell Proliferation Assay (Promega) as described<sup>22</sup>. Initial screens were performed in the presence of 80  $\mu$ M compound with the trypanocidal activity scored as active, moderate or inactive when the % viable cells was <25%, between 25% and 75%, or >75%, respectively. For active structures, parasite growth was evaluated using different compound concentrations (80 to 0.82  $\mu$ M) and from the resulting dose-response curve, a compound's  $EC_{50}^{Epi}$  established.

Growth inhibition assays against luciferase expressing *T. cruzi* amastigotes was performed as previously described<sup>26</sup>. Briefly, L6 (1500) cells in mammalian growth medium (100  $\mu$ L) were allowed to adhere to the base of each well for 6 hours. *T. cruzi* trypomastigotes (10,000 in 100  $\mu$ L mammalian growth medium) were then added to monolayer, and infections performed overnight at 37°C under 5% (v/v) CO<sub>2</sub>. The cultures were washed in growth medium to remove non-internalized parasites, treated with compound-containing fresh growth medium and subsequently incubated at 37°C under 5% (v/v) CO<sub>2</sub> for 72 hours. Growth medium was removed, the cells lysed in cell culture lysis reagent (Promega) and reporter levels determined using the Luciferase Assay kit (Promega). Luminescence was then measured using a Fluostar Omega plate reader (BMG Labtech) with this activity being proportional to the number of live cells.

## **Data analysis**

The HTS output was analyzed using Microsoft Office 365. JChem for Office was used for chemical database access, search and reporting (JChem for Office 16.8.2200). Analysis of the kinetic data, inhibition mechanism,  $IC_{50}$  and  $EC_{50}$  values were analyzed using GraphPad Prism 5 (GraphPad Software).

## Results

### Automated primary HTS

Recombinant TcMEc and TcMEem were purified and their kinetic parameters determined under the HTS assay conditions (Fig S1, S1 Table). The L-aspartate activation constant ( $K_A$ ) was determined for the recombinant TcMEc;  $K_A$  value =  $400 \pm 40$   $\mu$ M. Using this data, the ME coupled reaction was then optimized for the end-point HTS assay. Once appropriately adapted, the inhibitory effect of a diverse chemical library containing 29,760 structures was evaluated on each trypanosomal enzyme using a single concentration (20  $\mu$ M) of compound. Average Z-factor values were  $0.85 \pm 0.03$  and  $0.80 \pm 0.04$  for TcMEc and TcMEem, respectively. 631 ( $RA \leq 57.7\%$ ) and 478 ( $RA \leq 56.1\%$ ) hit candidates were identified for TcMEc and for TcMEem, respectively, with 287 molecules inhibiting both enzymes.

The hit candidates were transferred from the screening library plates to new assay plates and assayed in triplicate against ME coupled assay and against diaphorase, both in kinetic mode. Confirmed hits fulfilled the following criteria: ME inhibition ( $RA^{ME} \leq 50\%$ ), inactive against diaphorase ( $RA^{diaphorase} \geq 80\%$ ) and time independent inhibition (ME activity linear along the assay time). Following these criteria, 287 and 74 hits were confirmed for TcMEc and TcMEem, respectively, with 27 common for both enzymes.

### Kinetic characterization of hits

The most potent hits ( $RA^{ME} \leq 30\%$ ) together with 99 commercially available analogues, totalizing 308 molecules, were resupplied. This compound collection was then assayed

in triplicate against both TcMEs, the three HsMEs and diaphorase, at 80  $\mu\text{M}$ . The DNA fragments encoding for the catalytic regions of HsME1, HsME2 and HsME3 were heterologously expressed in *E. coli*, each enzyme purified and their kinetic parameters determined (S1 Table). These biochemical screens revealed that 262 compounds inhibited at least one of the *T. cruzi* MEs without affecting diaphorase activity: seven molecules were eliminated due to their inhibitory effect on diaphorase and 39 compounds did not inhibit TcMEs activity. For the ME specific inhibitors,  $\text{IC}_{50}$  values of each compound towards the TcMEs and HsMEs were determined (Fig 2, S2 Table). For TcME<sub>m</sub>, the  $\text{IC}_{50}$  values ranged from 0.5 to 71  $\mu\text{M}$  while for TcME<sub>c</sub> this varied from 0.0032 to 64  $\mu\text{M}$  (Fig S2). Many compounds in the “resupply” library also inhibited at least one of the human MEs although encouragingly some were inactive against all three mammalian isoforms. Based on their chemical backbone and ability to target the trypanosomal enzyme, the compounds that constitute the “resupply” library could be clustered into 6 structurally related different groups, designated as ATR1 to ATR6, with a seventh assemblage consisting of 12 non-structurally related singletons, designated as ATR7 (Fig 2).

To determine their mechanism of inhibition, a representative member from each structural group that generated an  $\text{IC}_{50}$  values  $\leq 10 \mu\text{M}$  (ATR2-001, ATR3-001, ATR4-001 and ATR5-001) was tested against TcME<sub>m</sub>: this isoform was used as unlike TcME<sub>c</sub>, its does not undergo allosteric activation thereby simplifying interpretation of the inhibition data. For ATR3-001 and ATR5-001, a mixed-type inhibition with respect to both substrates was noted (Fig S3). In contrast, TcME<sub>m</sub> activity in the presence of ATR2-001 resulted in a competitive inhibitory mechanism towards malate and mixed-type to  $\text{NADP}^+$

whereas ATR4-001-treated enzyme was competitive to malate and uncompetitive to NADP<sup>+</sup> (Fig S4).

### ***In vitro T. cruzi* antiproliferative assays**

To determine whether any of the TcME inhibitors displayed anti-parasitic properties, a selected subset of compounds were screened for trypanocidal activity against cultured *T. cruzi* epimastigotes. The compounds used were selected based on their IC<sub>50</sub> values towards the trypanosomal enzymes: The structures tested generated IC<sub>50</sub> <15 μM against one or both TcMEs (ATR1, 2, 4-7), while a range (20 out of 183) of ATR3 compounds that elicited IC<sub>50</sub> values ranging from 3 nM to 10 μM were screened. Out of the 44 agents examined, 13 displayed moderate trypanocidal effect at 80 μM with 21 having no significant effect on parasite growth at this concentration (S2 Table). For the remaining 10 active compounds (Fig 3), growth inhibition assays were conducted to determine their potency against epimastigote parasites, yielding EC<sub>50</sub><sup>Epi</sup> values ranging from 14 to 56 μM (Table 1). In parallel, benznidazole used as a control treatment, generated an EC<sub>50</sub><sup>Epi</sup> of 12 ± 1 μM. The biological activity of the 10 active compounds, was extended to evaluate their toxicity towards mammalian cells and *T. cruzi* amastigotes. Against the rat skeletal L6 line, 2 compounds (ATR5-001 and ATR7-005) had no effect on mammalian cell growth at concentrations up to 80 μM while the remaining 8 structures yielded EC<sub>50</sub><sup>L6</sup> values ranging from 14 to 55 μM (Table 1). When tested against *T. cruzi* amastigotes and using a single compound dosage at a concentration that did not affect host cell growth, 4 molecules (ATR3-128, ATR6-001, ATR7-005 and ATR7-008) displayed anti-parasitic activity, preventing growth of the intracellular pathogen by >90% relative to untreated controls (Table 1).



## Discussion

The TcMEs are a promising drug target for Chagas disease treatment, due to their importance in helping maintain NADPH levels in the *T. cruzi* parasite. In this study, using a biochemical HTS we evaluated approximately 30,000 compounds as potential TcMEs inhibitors. A total of 262 compounds were identified and confirmed as blocking this activity with the hits falling into 6 groups of structurally related molecules and a group with 12 singletons. The results obtained for each group is discussed below.

The 3 compounds that comprise the ATR1 group all contain a benzyl-xanthine core within their backbone (Fig 2), with this type of scaffold already described as inhibitors of human BRAF protein kinase<sup>27</sup>. Here, members of this family presented moderate inhibitory activity towards the TcMEs (IC<sub>50</sub> values of 12-48 μM) and HsME2 & 3 (IC<sub>50</sub> around 18 μM), with no effect on HsME1. For one of the ATR1s, ATR1-003, the presence of a sulfhydryl group attached to an imidazole ring on the xanthine backbone appears to underlie its mode of TcME inhibition: the ATR1-003 related compounds, ATR1-004 and ATR1-005, that contain a hydrogen or thiomethyl side chain at R1, have no affected enzyme function (Fig 4A). Unfortunately, none of the ATR1s screened against *T. cruzi* epimastigotes had any effect on parasite growth.

All 7 ATR2s, which contain a tetrazol-yl 4 quinolinecarboxamide or N-1H-tetrazol-5-yl-9H-xanthene-9-carboxamide core, proved to be general ME inhibitors targeting each parasite and mammalian isoform tested. Intriguingly, some of these compounds were up to ~5-fold more selective towards TcME<sub>m</sub> relative to the other enzymes. Despite only determining the IC<sub>50</sub> values of a limited number of ATR2s, it is clear that different ring-based substituents at the R1 position on the conserved quinoline does not affect a

compounds inhibition potency (Fig 4B): ATR2-004, ATR2-006 and ATR2-007 all exhibit similar  $IC_{50}$  values towards TcMEc or TcME<sub>m</sub> even though the former contains a tri-cyclic xanthene structure whereas the remaining two compounds possess a benzyl or thiophene moiety linked to the bicyclic quinolone ring. As with the ATR1 structures samples, no ATR2 compound displayed trypanocidal activity.

The ATR3 compounds are related in that they possess a sulfonamide linker that connects two aromatic rings (5 or 6 membered). A total of 218 structures were identified as inhibiting the trypanosomal MEs with most (212) only targeting TcMEc. Of these, many generated an  $IC_{50}$  below 100 nM with ATR3-007 yielding a value of 3.2 nM. When the potency of these compounds towards the human ME isoforms was examined, 189 had no effect on any of the mammalian enzymes further demonstrating the specificity of these inhibitors towards TcMEc. This way, a preliminary structure-activity relationship (SAR) analysis is presented for the most potent compounds, with  $IC_{50}$  values below 100 nM (Fig 5).

Despite the variety of chemical structures of the 27 ATR3 compounds yielding  $IC_{50}$  below 100 nM, 19 contain a nitrogen atom within a 6- or 5-membered ring, two ligations apart from N-sulfonamide. The addition of this nitrogen to ATR3-152, rendering ATR3-010, was sufficient to improve compounds potency by 912-fold. Less dramatic, but following the same behaviour, was the 5.8-fold gain in potency of compound ATR3-063, compared to ATR3-127. The addition of another nitrogen atom in the ring has deleterious effect for inhibitory activity, as seen in compound ATR3-055, that is 8.5-fold less potent than ATR3-026. Other orientations of the N-pyridinyl ring were found, as in ATR3-170 and ATR3-188 (nitrogen located 3 ligations apart from N-sulfonamide), and in ATR3-003,

ATR3-004 and ATR3-153 (nitrogen 4 ligations apart from N-sulfonamide), all these inhibitors exhibited IC<sub>50</sub> values in the micromolar range (S2 Table). Interestingly, ATR3-003 and ATR3-004 inhibited TcME<sub>m</sub> as well. In the subgroup of N-(2-pyridinyl)benzenesulfonamides (A = N, Fig 2), the following substituents in the pyridinyl ring were found: methyl at R7, R8 and R9 (also concomitantly at R7 and R9), and halogens (chlorine and bromine) at R8. However no compound with a substituent at R6 was identified. Analysing analogues of ATR3-020, the higher activity provided by the addition of chlorine at R8 is noteworthy. Likewise, from the 14 compounds of this subclass with an IC<sub>50</sub> values below 100 nM, 10 have a halogen atom at R8. Regarding the benzene region, different substituents were found at all the positions of the ring. For instance, halogens, alkyl, methoxy and ethoxy, including a fused ring (ATR3-007) as well as another ring connected by a carboxamide (ATR3-002) were recognized. The presence of a chlorine at R3 (ATR3-026) improved activity in at least 50-fold compared to trifluoromethoxy (ATR3-113) and amine (ATR3-157) (Fig 5).

Another representative ATR3 subgroup, presented among the most potent inhibitors, was formed by 4-(methylsulfanyl)-N-phenylbenzenesulfonamides (R3 = methylsulfanyl). Comparison of ATR3-028 analogues revealed the trend Br = Cl > F > Methyl > Methoxy for inhibitory activity, showing a preference for halogens at R8. The same occurs at position R7, where the replacement of methyl (ATR3-072) for chlorine (ATR3-028) improved potency by 10.8 fold. In the screened library, no compounds from this subgroup had substituents at positions R1, R2, R4 and R5. In contrast, within the subgroup of 4-(methoxy)-N-phenylbenzenesulfonamides (R3 = methoxy), inhibitors with halogens (chlorine, fluorine, iodine), methyl or amide at R2 were identified. Again, as seen for the

other subgroups, the presence of a halogen atom at R8 (ATR3-039 and ATR3-061 as compared to ATR3-150) increased the inhibitory activity in one order of magnitude. Beside these subgroups, 3 compounds with a benzoic acid connected to N-sulfonamide were active in concentrations in the nanomolar range (< 100 nM). The substitution of an acid group at R6 enhances 40-fold the potency (ATR3-130 – ATR3-017). The acid position in the ring affected dramatically the activity, as seen in compound ATR3-210, 2000-fold less potent than ATR3-017 (Fig 5).

In addition to being able to block TcMEc activity, ATR3 compounds also displayed anti-trypanosomal activity against epimastigote (ATR3-045, ATR3-073 and ATR3-128) and amastigote (ATR3-128) forms of *T. cruzi* (Table 1). Sulfonamide-based drugs are frequently used to treat various bacterial and protozoal infections, blocking dihydropteroate synthetase (DHPS) activity and therefore preventing folate synthesis. It is unlikely that the trypanocidal mode of action of the ATR3 structures identified here involves DHPS inhibition as *T. cruzi* is auxotrophic for folates and pterins<sup>28</sup>. Interestingly, sulfonamides similar to the ATR3 TcMEc inhibitors are also present in the reported GSK Chagas Box, a set of 222 lead-like molecules that came out of a phenotypic HTS using a library of 1.8 million compounds<sup>29</sup>. A preliminary assay of TcMEs against the GSK Chagas Box confirmed 3 sulfonamides as potent inhibitors of TcMEc (data not shown). These data, together with the results reported here, encourage further phenotypic studies with the ATR3 dataset to evaluate possible correlation between TcMEc inhibition and parasite death.

Out of all the TcMEs inhibitor hits, the pyrimidinone-based ATR4 compounds demonstrated the highest selectivity towards TcMEc. Two of these specifically blocked

the activity of this trypanosomal isoform, including one (ATR4-003) that displayed trypanocidal properties against *T. cruzi* epimastigotes (Table 1; Fig 3). Unfortunately, ATR4-003 also exhibited toxicity to mammalian cells and did not affect *T. cruzi* amastigote growth. This group displayed the best behaviour regarding the inhibition mechanism, which was competitive with respect to malate and uncompetitive with respect to NADP<sup>+</sup>. This feature indicates a sequential binding of NADP<sup>+</sup>, followed by the inhibitor, which occupies the malate site. Interestingly, ATR4-like compounds are reported to inhibit the 1-deoxy-D-xylulose-5-phosphate synthase from *Mycobacterium tuberculosis* (MtDXS)<sup>30</sup>. This enzyme participates in the mevalonate-independent, isoprenoid biosynthesis pathway utilizing pyruvate (ME product) and D-glyceraldehyde 3-phosphate to produce 1-deoxy-D-xylulose-5-phosphate<sup>31</sup>. As *T. cruzi* synthesizes isoprenoids *via* a mevalonate-dependent pathway<sup>32</sup> and apparently lacks a DXS homologue, it is unlikely that ATR4 targets this type of activity within cultured parasites.

The ATR5 group comprises 12 structures distinguished by the presence of an azatricyclo decenedione motif. Generally, they function as moderate TcMEM, TcMEc, HsME2 and HsME3 inhibitors, with none affecting HsME1 activity. Some compounds that affect both trypanosomal enzymes appear to show a degree of selectivity (~ 5- to 8-fold) towards TcMEM. One of the compounds (ATR5-001) that specifically targets TcMEM displays growth inhibitory activity against *T. cruzi* epimastigotes (EC<sub>50</sub><sup>Epi</sup> of 14.1 μM) (Table 1) while having no cytotoxic effect on mammalian cells. However, ATR5-001 was inactive against intracellular parasites. Compounds related to ATR5 have been reported to be inhibitors of thioredoxin glutathione reductase expressed by *Schistosoma mansoni*, with such structures being particularly effective against this parasites larva stage<sup>33</sup>.

The four active ATR6 molecules are of interest as they have no activity towards any of the HsMEs and displayed specific inhibition against TcME<sub>m</sub> (ATR6-001 and ATR6-004) or TcME<sub>c</sub> (ATR6-002 and ATR6-003) (Fig 2). The TcME<sub>m</sub> preference appears to be due to the presence of a heterocyclic ring (pyridine or morpholine) at position R1 while smaller side chains (amine or ethoxy) confers selectivity towards TcME<sub>c</sub> (Fig 4C). Encouragingly, ATR6-001 displays activity against *T. cruzi* epimastigotes and amastigotes. Given that very few members of compound group were tested, the generation of ATR6 derivatives will aid in understanding how this class of chemicals interact with TcME<sub>m</sub> or TcME<sub>c</sub>. This coupled with further phenotypic screens may lead to the identification of more potent trypanocidal ATR6 structures that exhibit low toxicity to mammalian cells.

In addition to the structurally related compounds, a total of 12 unrelated chemicals (singletons) were identified from the HTS as inhibiting TcME<sub>m</sub> and/or TcME<sub>c</sub> with these being assigned to the ATR7 group. Most showed TcME inhibition specificity (9 targeted only TcME<sub>c</sub> while 2 were specific for TcME<sub>m</sub>) with these structures having no effect on mammalian enzyme activity. Only 1 compound (ATR7-010) blocked the activity of both trypanosomal enzymes with this effect extending across to all mammalian counterparts. Out of the 12 ATR7 variants, the most promising were ATR7-005 and ATR7-008. These both showed activity against *T. cruzi* epimastigotes and amastigotes with the former having displayed no cytotoxic effect against mammalian cells at the highest concentration assayed (80  $\mu$ M).

The variety of compounds discovered here demonstrates that TcMEs are amenable to drug-like compounds inhibition. This is an essential feature of a drug target, and the *T. cruzi* MEs were assessed for the first time in this context. An intriguing feature

to emerge from this work stems from the high number of potent ( $IC_{50}$  values in nanomolar range) TcMEc specific inhibitors identified from the screens relative to those that target TcME<sub>m</sub>, indicating that cytosolic isoform may be more druggable than the mitochondrial variant. It is tempting to speculate that the higher availability of inhibitors targeting TcMEc may correlate with the presence of the allosteric site for aspartate. The fact that specific inhibitors for the two isoforms display trypanocidal effect suggests that both TcMEs may be essential for the parasite survival. Further experiments to assess target specificity of the identified molecules are required to confirm the essentiality of both TcME isoforms.

This work reports the first set of inhibitors against TcMEs in addition to the trypanocidal activity of these compounds towards the intracellular stage of this pathogen. This medically relevant developmental stage represents the most important target for anti-parasite therapies. Furthermore, new efforts in structural studies are required to identify the binding sites of the inhibitors on TcMEs molecules, especially regarding the compounds of ATR3 class. Besides, an expansion of the *in vitro* antitrypanosomal studies is also important to optimize the best trypanocidal drug. Lastly, also further studies to evaluate if the observed effects are due to an off target contribution will represent significant progress to defeat the neglected disease caused by this pathogen.

## **Acknowledgment**

We thank Paul A. M. Michels (University of Edinburgh, UK) for reviewing the manuscript and GlaxoSmithKline for the transfer of GSK Chagas Box compounds.

## **Funding**

This work was supported by Sao Paulo Research Foundation (FAPESP) (Process numbers: 2013/03983-5, 2012/23682-7 and 2015/03336-5).



## References

1. Rassi, A.; Marin-Neto, J. A. Chagas Disease. *Lancet* **2010**, *375*, 1388–402.
2. World Health Organization <http://www.who.int/mediacentre/factsheets/fs340/en/> (accessed Aug 29, 2016).
3. Bermudez, J.; Davies, C.; Simonazzi, A.; et al. Current Drug Therapy and Pharmaceutical Challenges for Chagas Disease. *Acta Trop.* **2016**, *156*, 1–16.
4. Hasslocher-Moreno, A. M.; do Brasil, P. E. A. A.; de Sousa, A. S.; et al. Safety of Benznidazole Use in the Treatment of Chronic Chagas' Disease. *J. Antimicrob. Chemother.* **2012**, *67*, 1261–1266.
5. Murta, S. M. F.; Gazzinelli, R. T.; Brener, Z.; et al. Molecular Characterization of Susceptible and Naturally Resistant Strains of *Trypanosoma cruzi* to Benznidazole and Nifurtimox. *Mol. Biochem. Parasitol.* **1998**, *93*, 203–214.
6. Teston, A. P. M.; Monteiro, W. M.; Reis, D.; et al. In Vivo Susceptibility to Benznidazole of *Trypanosoma cruzi* Strains from the Western Brazilian Amazon. *Trop. Med. Int. Heal.* **2013**, *18*, 85–95.
7. Molina, I.; Gómez i Prat, J.; Salvador, F.; et al. Randomized Trial of Posaconazole and Benznidazole for Chronic Chagas' Disease. *N. Engl. J. Med.* **2014**, *370*, 1899–908.
8. Bern, C. Chagas' Disease. *N. Engl. J. Med.* **2015**, *373*, 456–466.
9. Krauth-Siegel, R. L.; Comini, M. A. Redox Control in Trypanosomatids, Parasitic Protozoa with Trypanothione-Based Thiol Metabolism. *Biochim. Biophys. Acta* **2008**, *1780*, 1236–48.
10. Lee, S. H.; Stephens, J. L.; Englund, P. T. A Fatty-Acid Synthesis Mechanism Specialized for Parasitism. *Nat. Rev. Microbiol.* **2007**, *5*, 287–97.
11. Igoillo-Esteve, M.; Maugeri, D.; Stern, A. L.; et al. The Pentose Phosphate Pathway in *Trypanosoma cruzi*: A Potential Target for the Chemotherapy of Chagas Disease. *An. Acad. Bras. Cienc.* **2007**, *79*, 649–63.
12. Leroux, A. E.; Maugeri, D. a; Opperdoes, F. R.; et al. Comparative Studies on the Biochemical Properties of the Malic Enzymes from *Trypanosoma cruzi* and *Trypanosoma brucei*. *FEMS Microbiol. Lett.* **2011**, *314*, 25–33.
13. Leroux, A. E.; Maugeri, D. a; Cazzulo, J. J.; et al. Functional Characterization of NADP-Dependent Isocitrate Dehydrogenase Isozymes from *Trypanosoma cruzi*. *Mol. Biochem. Parasitol.* **2011**, *177*, 61–4.
14. Juan, S. M.; Segura, E. L.; Cazzulo, J. J. Purification and Some Properties of the NADP-Linked Glutamate Dehydrogenase from *Trypanosoma cruzi*. *Int. J. Biochem.* **1978**, *9*, 395–400.
15. Silva Paes, L.; Suarez Mantilla, B.; Julia Barison, M.; et al. The Uniqueness of the *Trypanosoma cruzi* Mitochondrion: Opportunities to Target New Drugs Against Chagas' Disease. *Curr. Pharm. Des.* **2011**, *17*, 2074–2099.
16. Tielens, A. G. M.; van Hellemond, J. J. Surprising Variety in Energy Metabolism within Trypanosomatidae. *Trends Parasitol.* **2009**, *25*, 482–90.
17. Allmann, S.; Morand, P.; Ebikeme, C.; et al. Cytosolic NADPH Homeostasis in Glucose-Starved Procyclic *Trypanosoma brucei* Relies on Malic Enzyme and the Pentose Phosphate Pathway Fed by Gluconeogenic Flux. *J. Biol. Chem.* **2013**, *288*, 18494–505.

18. Loebers, G.; Anthony, A.; Maurer-fogy, I.; et al. Human NAD + -Dependent Mitochondrial Malic Enzyme. *J. Biol. Chem.* **1991**, *266*, 3016–3021.
19. Loeber, G.; Maurer-Fogy, I.; Schwendenwein, R. Purification, cDNA Cloning and Heterologous Expression of the Human Mitochondrial NADP(+)-Dependent Malic Enzyme. *Biochem J* **1994**, *304*, 687–692.
20. Studier, F. W. Protein Production by Auto-Induction in High-Density Shaking Cultures. *Protein Expr. Purif.* **2005**, *41*, 207–234.
21. Hsieh, J.-Y.; Su, K.-L.; Ho, P.-T.; et al. Long-Range Interaction between the Enzyme Active Site and a Distant Allosteric Site in the Human Mitochondrial NAD(P)+-Dependent Malic Enzyme. *Arch. Biochem. Biophys.* **2009**, *487*, 19–27.
22. Mercaldi, G. F.; Ranzani, A. T.; Cordeiro, A. T. Discovery of New Uncompetitive Inhibitors of Glucose-6-Phosphate Dehydrogenase. *J. Biomol. Screen.* **2014**, *19*, 1362–1371.
23. Zhang, J.-H. A Simple Statistical Parameter for Use in Evaluation and Validation of High Throughput Screening Assays. *J. Biomol. Screen.* **1999**, *4*, 67–73.
24. Camargo, E. Growth and Differentiation in *Trypanosoma cruzi*. I. Origin of Metacyclic Trypanosomes in Liquid Media. *Rev Inst Med São Paulo* **1964**, *6*, 93–100.
25. Taylor, M. C.; Lewis, M. D.; Francisco, A. F.; et al. The *Trypanosoma cruzi* Vitamin C Dependent Peroxidase Confers Protection against Oxidative Stress but Is Not a Determinant of Virulence. *PLoS Negl. Trop. Dis.* **2015**, *9*, 1–17.
26. Bot, C.; Hall, B. S.; Bashir, N.; et al. Trypanocidal Activity of Aziridiny Nitrobenzamide Prodrugs. *Antimicrob. Agents Chemother.* **2010**, *54*, 4246–4252.
27. Luo, C.; Xie, P.; Marmorstein, R. Identification of BRAF Inhibitors through in Silico Screening. *J. Med. Chem.* **2008**, *51*, 6121–6127.
28. Cavazzuti, A.; Paglietti, G.; Hunter, W. N.; et al. Discovery of Potent Pteridine Reductase Inhibitors to Guide Antiparasite Drug Development. *Proc. Natl. Acad. Sci. U. S. A.* **2008**, *105*, 1448–1453.
29. Peña, I.; Pilar Manzano, M.; Cantizani, J.; et al. New Compound Sets Identified from High Throughput Phenotypic Screening against Three Kinetoplastid Parasites: An Open Resource. *Sci. Rep.* **2015**, *5*, 8771.
30. Mao, J.; Eoh, H.; He, R.; et al. Structure-Activity Relationships of Compounds Targeting *Mycobacterium tuberculosis* 1-Deoxy-D-Xylulose 5-Phosphate Synthase. *Bioorganic Med. Chem. Lett.* **2008**, *18*, 5320–5323.
31. Bailey, A. M.; Mahapatra, S.; Brennan, P. J.; et al. Identification, Cloning, Purification, and Enzymatic Characterization of *Mycobacterium tuberculosis* 1-Deoxy-D-Xylulose 5-Phosphate Synthase. *Glycobiology* **2002**, *12*, 813–820.
32. Cosentino, R. O.; Agüero, F. Genetic Profiling of the Isoprenoid and Sterol Biosynthesis Pathway Genes of *Trypanosoma cruzi*. *PLoS One* **2014**, *9*.
33. Li, T.; Ziniel, P. D.; He, P.; et al. High-Throughput Screening against Thioredoxin Glutathione Reductase Identifies Novel Inhibitors with Potential Therapeutic Value for Schistosomiasis. *Infect. Dis. Poverty* **2015**, *4*, 40.

## Tables

**Table 1: Compounds with trypanocidal effect.**

Compound	IC <sub>50</sub> (μM) <sup>#</sup>			EC <sub>50</sub> <sup>Epi</sup> (μM)	EC <sub>50</sub> <sup>L6</sup> [SC] (μM)	Amastigote activity
	TcME <sub>m</sub>	TcME <sub>c</sub>	HsMEs			
ATR3-045	>80.00	0.32 ± 0.01	53.00 ± 10.00 <sup>2</sup>	23 ± 6	36 ± 5 [12.8]	Inactive
ATR3-073	>80.00	0.87 ± 0.00	>80.00	14 ± 2	26 ± 3 [12.8]	Inactive
ATR3-128	>80.00	3.80 ± 0.06	>80.00	41 ± 8	54 ± 5 [32]	Active at 32 μM
ATR4-003	5.10 ± 0.50	>80.00	>80.00	48 ± 6	14 ± 1 [5.1]	Inactive
ATR5-001	10.00 ± 0.70	>80.00	>80.000	14 ± 1	> 80 [80]	Inactive
ATR6-001	13.00 ± 1.00	>80.00	>80.00	29 ± 5	55 ± 9 [32]	Active at 32 μM
ATR7-005	>80.00	5.70 ± 0.30	>80.00	56 ± 8	> 80 [80]	Active at 80 μM
ATR7-006	>80.00	6.30 ± 0.50	>80.00	33 ± 5	15 ± 2 [5.1]	Inactive
ATR7-008	>80.00	8.90 ± 0.90	>80.00	19 ± 1	53 ± 10 [32]	Active at 32 μM
ATR7-010	3.80 ± 0.10	7.60 ± 0.40	13.0 ± 1.00 <sup>1</sup> 9.70 ± 0.80 <sup>2</sup> 11.50 ± 0.50 <sup>3</sup>	39 ± 4	34 ± 2 [12.8]	Inactive

<sup>#</sup>IC<sub>50</sub> for TcME<sub>m</sub>, TcME<sub>c</sub>, HsME1<sup>(1)</sup>, HsME2<sup>(2)</sup> and HsME3<sup>(3)</sup> are shown. When the IC<sub>50</sub> value is different than >80 μM, the value and isoform is indicated.

The growth inhibitory effects of the selected compounds against cultured *T. cruzi* epimastigotes (EC<sub>50</sub><sup>Epi</sup>), towards the mammalian L6 line (EC<sub>50</sub><sup>L6</sup>) and against the amastigote are shown. In the EC<sub>50</sub><sup>L6</sup> column, the values in square brackets represents the safe concentration [SC], defined as the highest compound concentration assayed which displayed less than 10% cytotoxicity against L6. For the amastigote activity, compounds that at the SC inhibited parasite growth by >90% was deemed 'active'

## Figure Legends

**Figure 1: Schematic of high throughput screening assay and workflow.** A: The activities of the malic enzyme (ME) and diaphorase were coupled through the formation/utilization of NADPH. In this system, malate is converted to pyruvate in a reaction catalyzed by NADP<sup>+</sup>-dependent ME. The resultant NADPH is then utilized by diaphorase to reduce resazurin to resorufin resulting in the reformation of NADP<sup>+</sup>. Resorufin formation can be followed by following the change in fluorescence. B: Flowchart diagram of HTS and characterization of hits. For more details, see Materials and Methods.

**Figure 2: Scaffold of TcMEs inhibitors groups.** TcME inhibitors were clustered into 6 structurally related groups (ATR1-6). The distinguishing chemical motifs and number (n) of compounds for each grouping are shown. The potency range (as judge by IC<sub>50</sub>) and number of compounds (in parentheses) targeting the trypanosomal (TcMEc; TcME<sub>m</sub>) and/or human (HSME1; HsME2; HsME3) are given. Compounds were deemed inactive if no IC<sub>50</sub> could be determined over the concentration range used (highest assayed concentration was 80 μM. \* Scaffold representative of 80% of ATR3 compounds. Within this group compounds are also found with substituted 5-membered heterocycles attached at the nitrogen of sulfonamide (10% of compounds), beside other substituents connected to sulfonamide, as aliphatic groups.

**Figure 3: Structure of TcME inhibitors used in phenotypic screens.** Selected compounds were assayed against *T. cruzi* epimastigote and amastigote forms (Materials and Methods). Values of EC<sub>50</sub> are presented in Table 1.

**Figure 4: SAR of groups ATR1, ATR2 and ATR6.** A: Comparison among ATR1 compounds shows the essentiality of a sulfhydryl group at position R1 for activity. B: SAR for ATR2 group shows that different ring systems are allowed without affecting potency against TcME<sub>m</sub>. C: SAR for ATR6 group. The presence of a ring system at position R1 gives selectivity against TcME<sub>m</sub>, while the substitution for an amine or methoxy changes the selectivity towards TcME<sub>c</sub>. When IC<sub>50</sub> is assigned as > 80 μM, it means that no compound could inhibit at least 50% the enzyme activity at 80 μM (the highest assayed concentration).

**Figure 5: SAR of ATR3 group.** In grey background, the most potent compounds (IC<sub>50</sub> < 10 nM) together with other representatives of inhibitors with IC<sub>50</sub> below 100 nM. The IC<sub>50</sub> presented is for TcME<sub>c</sub>. The arrows indicate the related compounds from a SAR series. The variable position among the analogues is highlighted for each serie.

Figure 1:

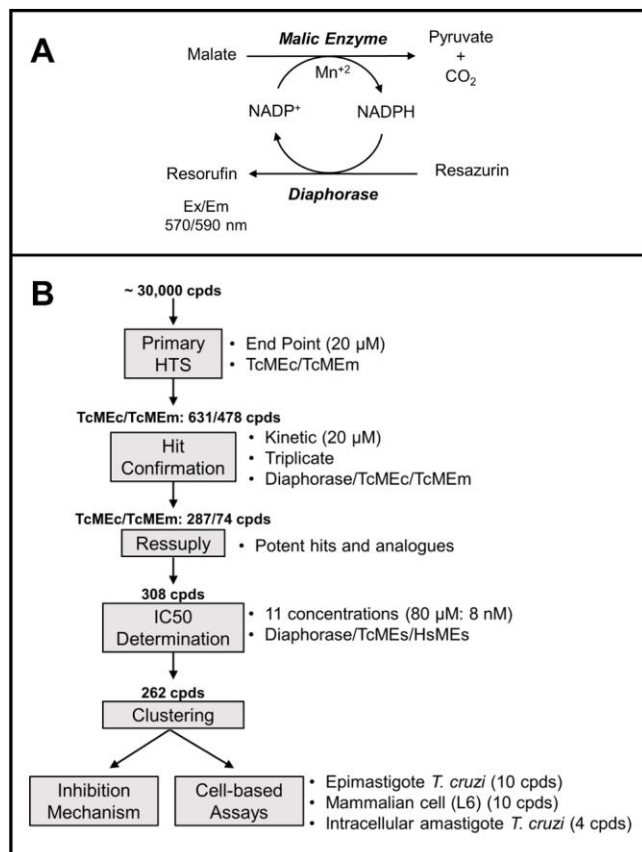
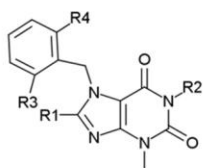
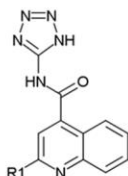


Figure 2:



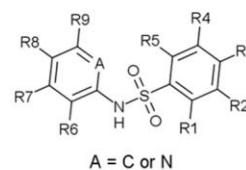
**Benzil-Xanthine**  
**ATR1 (n = 3)**

TcMEc: 26 - 48  $\mu\text{M}$  (3)  
TcMEem: 12 - 33  $\mu\text{M}$  (3)  
HsME1: Inactive  
HsME2: 14 - 19  $\mu\text{M}$  (3)  
HsME3: 10 - 16  $\mu\text{M}$  (3)



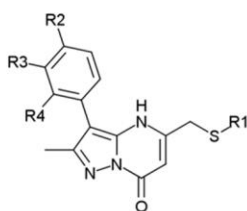
**Tetrazol 5-yl 4-quinolinecarboxamide**  
**ATR2 (n = 7)**

TcMEc: 3 - 25  $\mu\text{M}$  (7)  
TcMEem: 0.5 - 3.3  $\mu\text{M}$  (7)  
HsME1: 3.4 - 23  $\mu\text{M}$  (7)  
HsME2: 1.7 - 7  $\mu\text{M}$  (7)  
HsME3: 2.3 - 24  $\mu\text{M}$  (7)



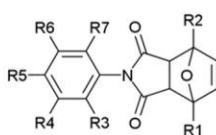
**Sulfonamides\***  
**ATR3 (n = 218)**

TcMEc: 0.003 - 58  $\mu\text{M}$  (218)  
TcMEem: 17 - 48  $\mu\text{M}$  (6)  
HsME1: Inactive  
HsME2: 5.7 - 77  $\mu\text{M}$  (22)  
HsME3: 2.3 - 76  $\mu\text{M}$  (12)



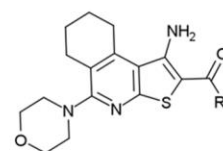
**Pyrimidin-7-one**  
**ATR4 (n = 6)**

TcMEc: 24 - 52  $\mu\text{M}$  (3)  
TcMEem: 2.4 - 43  $\mu\text{M}$  (6)  
HsME1: 6.8 - 11  $\mu\text{M}$  (3)  
HsME2: Inactive  
HsME3: 27 - 57  $\mu\text{M}$  (3)



**Azatricyclo decenedione**  
**ATR5 (n = 12)**

TcMEc: 35 - 64  $\mu\text{M}$  (7)  
TcMEem: 10 - 71  $\mu\text{M}$  (12)  
HsME1: Inactive  
HsME2: 9.2 - 51  $\mu\text{M}$  (6)  
HsME3: 6.3 - 36  $\mu\text{M}$  (9)



**Tetrahydrothieno isoquinoline**  
**ATR6 (n = 4)**

TcMEc: 17 - 50  $\mu\text{M}$  (2)  
TcMEem: 13 - 70  $\mu\text{M}$  (2)  
HsME1: Inactive  
HsME2: Inactive  
HsME3: Inactive

Figure 3:

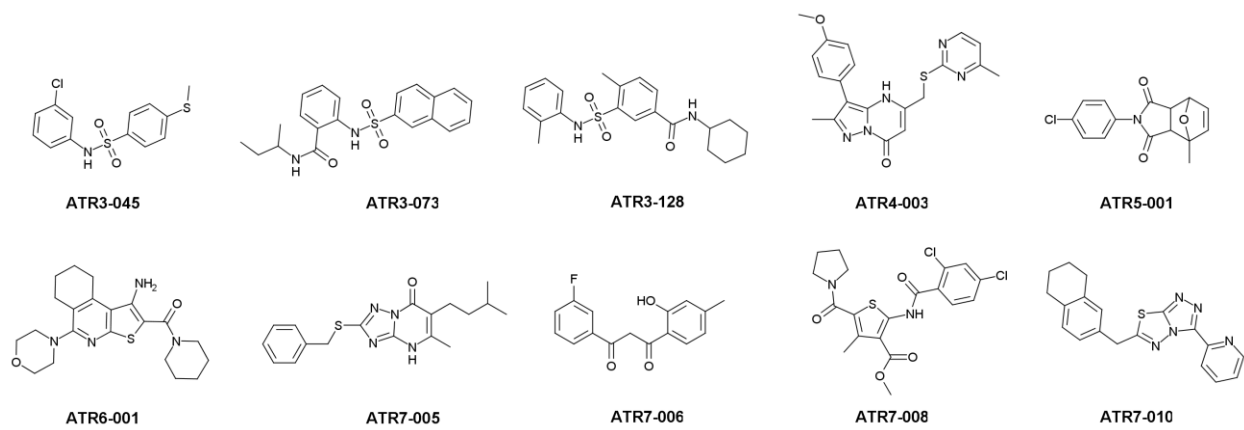




Figure 4:

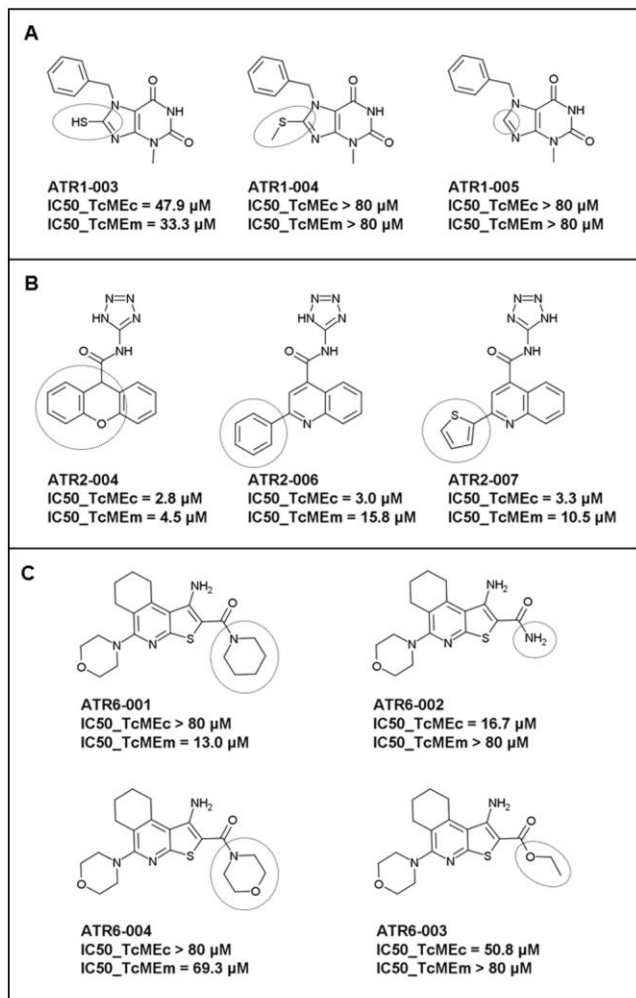


Figure 5:

